NEURAL REGENERATION RESEARCH
www.nrronline.org

Research Article

Photobiomodulation inhibits the expression of chondroitin sulfate proteoglycans after spinal cord injury via the Sox9 pathway

Zhihao Zhang, Zhiwen Song, Liang Luo, Zhijie Zhu, Xiaoshuang Zuo, Cheng Ju, Xuankang Wang, Yangguang Ma, Tingyu Wu, Zhou Yao, Jie Zhou, Beiyu Chen, Tan Ding, Zhe Wang*, Xueyu Hu*

https://doi.org/10.4103/1673-5374.374136

Date of submission: November 14, 2022

Date of decision: January 19, 2023

Date of acceptance: March 4, 2023

Date of web publication: April 20, 2023

From the Contents

Graphical Abstract

Photobiomodulation improves spinal cord injury outcome by reducing chondroitin sulfate proteoglycan expression via the Sox9 pathway in astrocytes

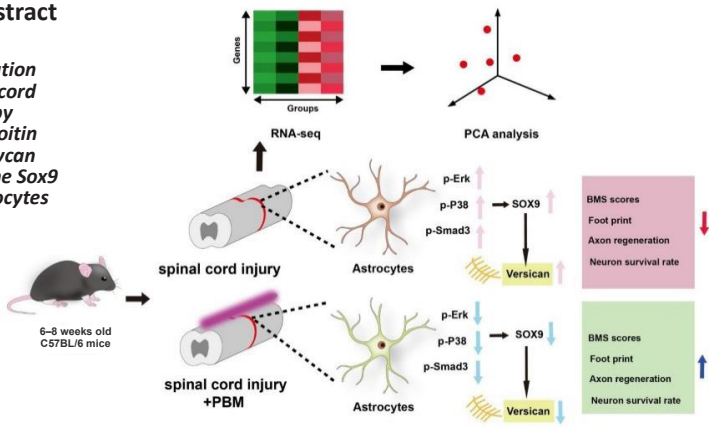

Abstract

Both glial cells and glia scar greatly affect the development of spinal cord injury and have become hot spots in research on spinal cord injury treatment. The cellular deposition of dense extracellular matrix proteins such as chondroitin sulfate proteoglycans inside and around the glial scar is known to affect axonal growth and be a major obstacle to autogenous repair. These proteins are thus candidate targets for spinal cord injury therapy. Our previous studies demonstrated that 810 nm photobiomodulation inhibited the formation of chondroitin sulfate proteoglycans after spinal cord injury and greatly improved motor function in model animals. However, the specific mechanism and potential targets involved remain to be clarified. In this study, to investigate the therapeutic effect of photobiomodulation, we established a mouse model of spinal cord injury by T9 clamping and irradiated the injury site at a power density of 50 mW/cm^2 for 50 minutes once a day for 7 consecutive days. We found that photobiomodulation greatly restored motor function in mice and downregulated chondroitin sulfate proteoglycan expression in the injured spinal cord. Bioinformatics analysis revealed that photobiomodulation inhibited the expression of proteoglycan-related genes induced by spinal cord injury, and versican, a type of proteoglycan, was one of the most markedly changed molecules. Immunofluorescence staining showed that after spinal cord injury, versican was present in astrocytes in spinal cord tissue. The expression of versican in primary astrocytes cultured *in vitro* increased after inflammation induction, whereas photobiomodulation inhibited the expression of versican. Furthermore, we found that the increased levels of p-Smad3, p-P38 and p-Erk in inflammatory astrocytes were reduced after photobiomodulation treatment and after delivery of inhibitors including FR 180204, (E)-SIS3, and SB 202190. This suggests that Smad3/Sox9 and MAPK/Sox9 pathways may be involved in the effects of photobiomodulation. In summary, our findings show that photobiomodulation modulates the expression of chondroitin sulfate proteoglycans, and versican is one of the key target molecules of photobiomodulation. MAPK/Sox9 and Smad3/Sox9 pathways may play a role in the effects of photobiomodulation on chondroitin sulfate proteoglycan accumulation after spinal cord injury.

Key Words: chondroitin sulfate proteoglycans; Erk; MAPK; P38; photobiomodulation; principal component analysis; Smad3; Sox9; spinal cord injury; versican

Introduction

Spinal cord injury (SCI) can cause severe permanent motor, sensory, and autonomic loss in adult mammals, mainly because of the difficulty of neuron regeneration and reconstruction of functional connections (Hutson and Di Giovanni, 2019). Chondroitin sulfate proteoglycans (CSPGs) accumulate in and around scars after SCI and are one of the main inhibitory factors in axonal regeneration (Mukherjee et al., 2020; Hu et al., 2022; Yu et al., 2022). After SCI, cells form glia scar by depositing dense extracellular matrix proteins such as CSPGs, which regulate the proliferation and survival of neurons by activating protein tyrosine phosphatase receptors including LAR and PTPσ. Therefore, much attention has been paid to reducing the growth inhibitory properties of CSPGs in recent years (Tran et al., 2018; Bradbury and Burnside, 2019). Previous studies have shown that chondroitin sulfate ABC (ChABC) modifies central nervous system (CNS) plasticity and promotes functional recovery by breaking down the glycosaminoglycan side chain of CSPGs (Moon et al., 2001; Bradbury et al., 2002). However, because of the challenges in protein stability (Khalil et al., 2022), and as the regulating pathways that contribute to the accumulation of CSPGs are complicated and yet to be clarified (Sofroniew and Vinters, 2010), limited success has been achieved on *in vivo* application of ChABC for down-regulation of CSPGs. Therefore, new strategies targeting CSPGs are needed.

Photobiomodulation (PBM) treatment, also called low-energy laser therapy, has been shown to act on mitochondria to improve ATP production, decrease the expression of reactive oxygen species (ROS), and regulate transcription factors (Chung et al., 2012). It has been widely used for treatment of multiple diseases because it has advantages of convenience of use, few adverse effects, and low cost (Chow et al., 2009; Lorenzini et al., 2010). In recent decades, its therapeutic role in degenerative and traumatic pathological CNS diseases

Department of Orthopedics, Xijing Hospital, Fourth Military Medical University, Xi'an, Shaanxi Province, China
***Correspondence to:** Zhe Wang, MD, wangzhe@fmmu.edu.cn; Xueyu Hu, MD, huxueyu@fmmu.edu.cn.
https://orcid.org/0000-0003-0852-1196 (Xueyu Hu); https://orcid.org/0000-0002-7573-1583 (Zhe Wang)

Funding: *This study was supported by the National Natural Science Foundation of China, Nos. 81070996 (to ZW), 81572151 (to XH); Shaanxi Provincial Key R&D Program, Nos. 2020ZDLSF02-05 (to ZW), 2021ZDLSF02-10 (to XH); Everest Project of Military Medicine of Air Force Medical University, No. 2018RCFC02 (to XH); and Boosting Project of the First Affiliated Hospital of Air Force Medical University, No. XJZT19Z22 (to ZW).*

How to cite this article: *Zhang Z, Song Z, Luo L, Zhu Z, Zuo X, Ju C, Wang X, Ma Y, Wu T, Yao Z, Zhou J, Chen B, Ding T, Wang Z, Hu X (2024) Photobiomodulation inhibits the expression of chondroitin sulfate proteoglycans after spinal cord injury via the Sox9 pathway. Neural Regen Res 19(1):180-189.*

has received much attention (Salehpour et al., 2018). Previous studies have shown that PBM modulated immune responses, alleviated inflammation, and promoted repair and regeneration after SCI (Wang et al., 2021b; Ma et al., 2022). These findings suggest that PBM has a potential therapeutic value for patients (Liang et al., 2022). Our previous study showed that 810 nm PBM treatment inhibits the accumulation of CSPGs after SCI in mice, accompanied by a reduction of inflammatory response and recovery in motor function (Sun et al., 2020). However, the specific mechanism by which PBM inhibits CSPGs after SCI has not been determined.

Sox9 is an important transcription factor that plays a key role in sex determination, chondrogenesis, and nerve injury repair in mammals (Eggers et al., 2014; Yang and Yan, 2022). Sox9 has been shown to mediate the upregulation of CSPG expression (Gris et al., 2007; McKillop et al., 2013) and regulate the expression of XT-1, C4ST, and CSPG core proteins including brevican, neurocan and aggrecan after SCI (McKillop et al., 2013). Smad3 and MAPK pathways are associated with the formation of CSPGs and contribute to the function of Sox9 (Jahr et al., 2019; Li et al., 2019). Smad3 is associated with Sox9 in the TGF-β-dependent regulation of scar accumulation. They form a transcription complex and bind to the enhancer region of Col2α. Activation of P38 also plays a role in stabilizing Sox9 mRNA, which can increase the level of Sox9 (Tew and Hardingham, 2006).

In the current study, we investigated the effect of PBM on the production of CSPGs after SCI. We also explored the potential mechanism of PBM-mediated regulation of CSPG production and the possible involvement of the Smad3/Sox9 and MAPK/Sox9 pathways.

Methods

Animals

Male C57BL/6 mice (*n* = 323, specific-pathogen-free level, 6–8 weeks old, weighing approximately 20 g) and newborn C57BL/6 mice (*n* = 30, 0–2 days old) were obtained from the Laboratory Animal Center of Fourth Military Medical University (Air Force Medical University, Xi'an, China) (license No. SCXK (Shaan) 2019-001). The animals were housed in warm, dry cages (*n* = 3 mice per cage) with a controlled ambient temperature of 22–24°C and relative humidity of 45–65% in a 12-hour diurnal cycle and provided with adequate food and water. The Ethics Committee of the Fourth Military Medical University reviewed the experimental protocol and approved the use of animals (approval IACUC No. 20210452, approval date: March 1, 2021). The animal experiments were performed in accordance with the Animal Research: Reporting of *In Vivo* Experiments (ARRIVE) guideline (Percie du Sert et al., 2020). All surgical, irradiation, and invasive procedures were carefully designed to reduce the number of animals used, and the mice were anesthetized beforehand to alleviate pain. The 323 adult male mice were randomly divided into sham (*n* = 27), SCI (*n* = 130), SCI + PBM (*n* = 130), SCI + inhibitors (*n* = 18), and SCI + PBM + inhibitors (*n* = 18) groups. The experimental overview is shown in **Figure 1A**.

Construction of the SCI model

The animals were acclimatized for a fortnight in advance and then a standard bilateral forceps compressive model was generated following a previous study (Ma et al., 2022). The mice were anesthetized before surgery by intraperitoneal injection of 0.6% sodium pentobarbital (10 mL/kg, Merck, Monmouth Junction, NJ, USA). After preparation and disinfection, the skin, subcutaneous tissue, and muscle were incised layer by layer. The spine and lamina of T9 vertebrae were removed with microsurgical scissors. The spinal cord was exposed and then clamped using a Dumont ligature forceps (Fine Scientific Tools, Heidelberg, Germany) modified with a metal spacer placed between blades to leave a 0.3 mm gap at the end of the forceps after closure. The modified forceps were inserted vertically, placed on both sides of the spinal cord, and clamped for 30 seconds. When the mice are clamped, the forceps closure is limited by the metal spacer, and SCI occurs from the instantaneous squeeze; this reduces the influence of the strength of the hand when squeezing the forceps, thus ensuring the appropriate degree of injury. During clamping, mice were observed to exhibit bilateral lower limb stretching and tail wagging, which indicates successful clamping. Bruising was observed on the spinal cord surface at the clamping site. The muscle layer and the skin were sutured and the wound was disinfected with iodophor. In the sham group, the T9 vertebral plate was opened to expose the spinal cord tissue without clamping. Laser fibers were implanted simultaneously in mice as described below. After surgery, the mice were resuscitated individually in a dry, warm cage. The bladders of the mice were massaged twice daily to promote urination and prevent the development of urinary tract infections. Animals with lower limb edema, injuries, and infected wounds were not included in the following experiment.

PBM irradiation

In this study, we used a laser fiber to provide SCI mice with implanted laser irradiation. The cylindrical fibers had a diameter of 600 μm with a biocompatible transparent medical silica layer on their surface to protect the fibers without weakening their optical properties. As described in a previous study (Ma et al., 2022), the front end of the medical scattering laser fiber (Xi'an Laser Technology Medical Technology Co., Ltd., Xi'an, China) was fixed to the muscle and soft tissue near the T8 cone with absorbable sutures after SCI, and the light-emitting portion of laser fiber was positioned above the spinal cord clamping injury site. The fiber optic was secured to the end of the skin wound outside of the mouse and a protective device was added to prevent gnawing by other mice.

Before irradiation, mice were anesthetized by intraperitoneal injection of 0.6% sodium pentobarbital (10 mL/kg). The anesthetized mice were placed in a warm, dark cage and the laser fiber was connected to an 808 nm semiconductor laser transmitter (MW-GX-808, LeiShi Optoelectronics Co., Ltd., Changchun, China). The mice were irradiated following the parameters used in a previous study (Ma et al., 2022); the detailed irradiation parameters are shown in **Additional Table 1**. The mice in PBM groups were irradiated at a power density of 50 mW/cm^2 in the SCI region for 50 minutes once a day; the first irradiation was provided in 30 minutes after surgery, and mice were irradiated in the following 7 days after injury. Animals were assessed for 28 days after injury (**Figure 1A**). Mice in other groups were implanted with a laser fiber and anesthetized each day, but the laser transmitter was not turned on. The actual output power of the fibers was tested before irradiation each time using a calibrated optical sensor to ensure that the output power fit.

Isolation and culture of astrocytes

Primary astrocytes were extracted from the cortex of newborn C57BL/6 mice (0–2 days) after isoflurane anesthesia, as described in a previous study (Wang et al., 2021b). The cerebral cortex was removed, and the meninges and venous plexus were removed. The cortex was cut into 0.5 mm thick slices; the slices were placed in 0.25% trypsin ethylenediaminetetraacetic acid (EDTA) solution (Solarbio, Beijing, China) at 37°C and gently shaken for 20 minutes. The digested tissue was neutralized and suspended in Dulbecco's modified Eagle medium/Nutrient mixture F-12 culture medium (DMEM/F12; HyClone, Logan, UT, USA) with 10% fetal bovine serum (Biological Industries, Beit HaEmek, Israel). The cell suspension was filtered with 100 nm nylon mesh (Falcon, Shmeissani, Amman, Jordan) and centrifuged for 5 minutes (1000 × *g*). Cells were resuspended in DMEM/F12 containing 10% fetal bovine serum and moved into T75 culture bottles coated with poly L-lysine (Thermo Fisher Scientific, Waltham, MA, USA). Cells were cultured in DMEM/F12 with 10% fetal bovine serum, penicillin (100 U/mL, New Cell Molecular Biotechnology Co., Ltd., Suzhou, Jiangsu, China), and streptomycin (100 μg/mL, New Cell Molecular Biotechnology Co., Ltd.). The culture medium was replaced on the first day after seeding and then replaced every 3 days. After 12–14 days of culture, the culture medium was changed; the bottle was shaken on a shaking table at 200 × *g* for 24 hours. The astrocytes at the bottom of the bottle were collected for subculture using trypsin. Cells were incubated in a humidified incubator containing 5% CO_2 at 37°C. Cells were identified by staining with glial fibrillary acidic protein (GFAP; a marker for astrocytes).

Cell treatments

To induce the inflammatory phenotype of astrocytes, cells were incubated with complement component 1q (C1q) (400 ng/mL, MyBioSource, San Diego, CA, USA), tumor necrosis factor-α (TNF-α) (30 ng/mL, Cell Signaling Technology, Danvers, MA, USA), and interleukin-1α (IL-1α) (3 ng/mL, Sigma, Waltham, MA, USA) as previously described (Wang et al., 2021b). Cells were irradiated with PBM (**Additional Table 1**) after inflammation induction, as reported previously (Wang et al., 2021b; Ma et al., 2022). The transcript levels of versican molecules were detected after inflammatory induction for 12 hours, and protein levels were detected after 24 hours.

To inhibit Erk, Smad3, and P38 pathways, astrocytes were pre-treated with FR 180204 (S7524, Selleck, Houston, TX, USA, 2 μg/mL) for 1 hour, (E)-SIS3 (HY-13013, MCE, Monmouth Junction NJ, USA, 5 μg/mL) for 1 hour, or SB 202190 (HY-10295, MCE, 7 μg/mL) for 30 minutes, respectively. The medium was replaced and inflammatory induction was performed. PBM treatment was delivered as described above. At 6 and 12 hours after induction, western blot was performed.

Functional analyses

The Basso Mouse Scale (Basso et al., 2006) was used to assess the recovery of motor function in the hind limbs of mice after SCI, with a score of 0–9 representing complete paralysis to normal movement. The scale was used to assess items such as the movement of the hind limb joints, the position of trunk, body stability, coordination of the forelimbs and hind limbs, paw position, toe clearance and tail position. The mice were trained and scored 2 weeks before the injury and then at 1, 3, 7, 14, 21 and 28 days after surgery. All scores were measured independently by two researchers blinded to animal grouping.

The recovery of motor function in mice after SCI was also assessed using gait analysis (Ma et al., 2001). Analysis was performed by dipping the forefoot and hindfoot with edible non-toxic blue and red dyes, respectively, and the mice were trained to walk over white paper to record the foot impressions. Mice were trained to pass through a special canal prior to injury and tested before injury and on 28 days after injury. Each mouse was tested twice and the step length was measured.

Mechanical allodynia was measured using von Fery filaments on day 7 post-injury. Mice were acclimated to the environment for 30 minutes prior to each trial. Temperature and humidity were kept constant during the experiment. Pain sensitivity in mice was assessed by two observers who were blinded to the grouping. To assess skin sensitivity to mechanical nociception, the soles of the bilateral hindlimbs of mice were stimulated with fibers of different intensities as described previously (Gaudet et al., 2021; Kong et al., 2021). The thresholds of 50% foot reduction in both hind feet were recorded as the values of mechanical nociceptive sensitivity.

Tissue analysis
Mice were intraperitoneally anesthetized with 0.6% sodium pentobarbital (10 mL/kg). The thorax was opened to expose the heart, cut the right atrial appendage and perfused from the left ventricle with saline. When the effluent was clear, the spinal cord (1.0 cm long, injury site located in the center of tissue) was dissected. For tissues used for sectioning, mice were slowly perfused with 4% paraformaldehyde after a sufficient saline perfusion as described above; the spinal cord was dissected and a 1.0 cm long section of spinal cord tissue (injury site located in the center of tissue) was soaked overnight in paraformaldehyde. The sample was then soaked in 25% sucrose solution at 4°C; the ventral side of the dehydrated tissue was placed on a tray and wrapped in optimal cutting temperature compound (OCT) on the freezing table. After the compound had solidified, sections (8 μm thick) were cut with a microtome (CM1900, Leica, Wetzlar, Hesse, Germany) in the sagittal plane of the spinal cord; the tissue near the central aqueduct was sectioned continuously.

Western blot analysis
Spinal cord tissue and cells were lysed in radioimmunoprecipitation assay (RIPA, Beyotime, Shanghai, China) lysis buffer supplemented with protease and phosphatase inhibitors (MCE), followed by centrifugation. After the addition of 5× sodium dodecyl sulfate, the samples were boiled in a metal bath at 100°C for 15 minutes. Protein concentrations were determined using the bicinchoninic acid method (Walker, 1994). Equal concentrations of protein (30–50 μg) were separated on a 4–20% SurePAGE gel (Genscript, Nanjing, Jiangsu, China) and transferred to nitrocellulose (NC) membrane (Pall, New York, NY, USA). The membranes were soaked in 5% skimmed milk for 1 hour at room temperature and incubated overnight at 4°C with the following primary antibodies: anti-mouse glyceraldehyde-3-phosphate dehydrogenase (GAPDH) (1:3000, Proteintech, Wuhan, Hubei, China, Cat# 60004-1-Ig, RRID: AB_2107436), anti-mouse chondroitin sulfate proteoglycans (CSPG) (1:1000, Sigma-Aldrich, St. Louis, MO, USA, Cat# C8035, RRID: AB_476879), anti-mouse versican (1:1000, Thermo Fisher Scientific, Cat# S351-23, RRID: AB_2735409), anti-rabbit Sox9 (1:1000, Abcam, Cambridge, UK, Cat# ab185966, RRID: AB_2728660), anti-rabbit p-P38 MAPK (P38) (1:1000, CST, Danvers, MA, USA, Cat# D3F9, RRID: AB_2139682), anti-rabbit P38 (1:1000, CST, Cat# D13E1, RRID: TSC_SD02390), anti-rabbit p-extracellular signal-regulated kinase 1/2 (Erk1/2) (1:1000, CST, Cat# D13.14.4E, RRID: AB_10694057), anti-rabbit Erk1/2 (1:1000, CST, Cat# 137F5, RRID: AB_10693607), anti-rabbit p-Smad3 (1:1000, CST, Cat# C25A9, RRID: AB_2193207), anti-rabbit Smad2/3 (1:1000, CST, Cat# D7G7, RRID: AB_10889933), anti-rabbit p-c-Jun N-terminal kinase (JNK) (1:1000, Proteintech, Cat# 80024-1-RR, RRID: AB_2882943), and anti-rabbit JNK (1:1000, Proteintech, Cat# 66210-1-Ig, RRID: AB_2881601). The bands were washed three times with Tris buffer solution-Tween (TBST) and incubated with the corresponding secondary antibodies (goat anti-rabbit horseradish peroxidase antibody, 1:3000, InCellGene, San Antonio, TX, USA, Cat# SA-10011; goat anti-mouse horseradish peroxidase antibody, 1:3000, InCellGene, Cat# SA-10010) at 37°C for 1 hour. The bands were developed using Western SuperSensitive Substrate (InCellGene) and images were acquired using an Amersham Imager 600 luminometer (GE Healthcare, Stockholm, Sweden). The optical densities of bands were measured using ImageJ software (v1.4.67; National Institutes of Health Bethesda, MD, USA) (Schneider et al., 2012).

Immunofluorescence staining
Frozen spinal cord tissue sections or formaldehyde-fixed cultured astrocytes were rinsed three times with ice-phosphate buffer and then incubated with 1% donkey serum containing 0.3% Triton X-100 for 30 minutes. Sections or cells were incubated overnight at 4°C with the following primary antibodies: anti-GFAP (chicken, 1:400, Abcam, Cat# ab4674, RRID: AB_304558), anti-CSPG (mouse, 1:200, Sigma-Aldrich, Cat# C8035, RRID: AB_476879), anti-versican (mouse, 1:200, ThermoFisher, Cat# S351-23, RRID: AB_2735409), anti-microtubule associated protein 2 (MAP2; mouse, 1:200, CST, Cat# D5G1, RRID: AB_10829170), and anti-NeuN (mouse, 1:200, Abcam, Cat# ab104224, RRID: AB_10711040). Sections and cells were washed three times and incubated for 1 hour at 37°C with corresponding secondary antibodies (Goat anti-Mouse IgG (H+L) Cross-Adsorbed Secondary Antibody, Alexa Fluor 594, goat, 1:200, Invitrogen, Waltham, MA, USA, A-11005, RRID: AB_141372; Goat anti-Chicken IgY (H+L) Secondary Antibody, Alexa Fluor 488, goat, 1:200, Invitrogen, A-11039, RRID: AB_142924; Goat anti-Rabbit IgG (H+L) Cross-Adsorbed Secondary Antibody, Alexa Fluor 488, goat, 1:200, Invitrogen, A-11008, RRID: AB_143165; Goat anti-Rabbit IgG (H+L) Cross-Adsorbed Secondary Antibody, Alexa Fluor 594, goat, 1:200, Invitrogen, A-11012; RRID: AB_141359). After washing, the nuclei were stained using anti-fluorescence quencher containing 4′,6-diamidino-2-phenylindole (DAPI) (ThermoFisher). The number of surviving neurons was measured within 0.5 mm of the para-lesion area. Fluorescent images were acquired using a fluorescent microscope (BX51, Olympus, Tokyo, Japan) and fluorescence intensity was analyzed with ImageJ software.

Quantitative PCR
Total RNA was extracted from frozen mouse spinal cord tissue and cells using Trizol. Complementary DNA (cDNA) was reverse transcribed from RNA using Evo M-MLV RT Premix (AG11706, Accurate Biotechnology (Hunan) Co., Ltd., Suzhou, China) and stored at –20°C. cDNA was then amplified with the SYBR Green amplification system (Accurate Biotechnology (Hunan) Co., Ltd). qPCR data were analyzed using the $2^{-\Delta\Delta CT}$ method (Livak and Schmittgen, 2001); *β-actin* (housekeeping gene) was used as an internal reference gene to normalize gene expression. PCR primer sequences are listed in **Additional Table 2**.

RNA-sequencing
Total RNA was collected from the spinal cord tissues using the Trizol kit (Takara, Tokyo, Japan) 7 days after SCI. RNA quality was assessed using gel electrophoresis and a Nanodrop spectrophotometer (ThermoFisher). After mRNA enrichment, fragmentation, reverse transcription, library construction, and HiSeq X Ten operations, mRNA expression values were determined using the Cufflinks method (Ghosh and Chan, 2016). The above work was performed by Shanghai Jingneng Biotechnology Co. (Shanghai, China). $P \leq 0.05$ indicated statistical significance.

Proteoglycan-related genes were analyzed in two steps. First, to verify the effect of PBM on the expression of proteoglycan-related molecular profiles, principal component analysis was performed on genes measured in RNA-sequencing. We adopted the Screen plot and principal component (PC) over-determination (which must satisfy the criterion that at least two |factor loadings| no less than 0.6) to confirm PCs. Variables in one PC that have a strong interrelationship would have a high loading score. The distribution of variables in PC1 and PC2 was recognized with two-dimensional image (Awai et al., 2016). Next, the expression of genes was individually validated using RNA-seq data and qPCR to identify the molecules that were most significantly interfered by PBM.

Pharmacological interventions
For the inhibitor treatments (SCI + PBM + inhibitors), 18 mice were randomly divided into SCI + FR 180204, SCI + SB 202190, and SCI + (E)-SIS3 groups (n = 6 mice for each group). FR 180204, SB 202190, and (E)-SIS3 were dissolved in dimethyl sulfoxide and normal saline, and mice were injected at 30 μg/kg, 5 mg/kg, and 44 μg/kg, respectively. SB 202190 and (E)-SIS3 solutions were intraperitoneally injected into the peritoneal cavity using a 1 mL sterile medical syringe once a day and FR 180204 was intraperitoneally injected once every 2 days.

Statistical analysis
No statistical methods were used to predetermine sample sizes; however, our sample sizes were similar to those reported in previous publications (Shen et al., 2009; Francos-Quijorna et al., 2022). No animals or data points were excluded from the analysis. All data are expressed as mean ± standard deviation (SD). Statistical analysis of the results was performed using GraphPad Prism (version 9.0.0, GraphPad Software, San Diego, CA, USA, www.graphpad.com). One-way analysis of variance with the least significance difference *post hoc* test was used for comparisons among different groups at the same time point, and multiple repeated measures analysis of variance with the least significance difference *post hoc* test was used for comparisons among treatment groups at different time points. $P \leq 0.05$ indicated statistical significance.

Results

PBM promotes motor function recovery after SCI in mice
The functional recovery of SCI model mice after PBM irradiation was evaluated using the Basso Mouse Scale score and footprint analysis (**Figure 1B–D**). PBM irradiation markedly increased Basso Mouse Scale scores in SCI model mice from day 7 post-injury, and this difference was maintained until day 28 (**Figure 1B**). Footprint analysis showed that the step length in the SCI group was markedly shorter than that in the Sham group at 28 days after injury, and the step length of the mice in the SCI + PBM group was longer compared with that in the SCI group (**Figure 1C** and **D**). We also measured the mechanical allodynia on day 7 post-injury, and the results showed that PBM markedly alleviated mechanical allodynia in SCI model mice (**Additional Figure 1**). These results indicate that PBM irradiation promoted the recovery of motor function in animals after SCI.

PBM reduces the expression of CSPGs after SCI in mouse spinal cord
A previous study reported that PBM markedly decreased the expression level of CSPGs in SCI model rats at 7 days post-injury (Sun et al., 2020), The effect of PBM irradiation on CSPGs was first evaluated by western blot assay (**Figure 2A** and **B**). CSPGs accumulated rapidly after injury, peaked at 7 days post-injury, and then gradually decreased over 28 days. PBM irradiation reduced the accumulation of CSPGs in the injured spinal cord; the expression of CSPGs was markedly reduced in the PBM irradiated group compared with the SCI group at 3, 7, 14, and 28 days post-injury. We assessed the effect of PBM irradiation on CSPG spatial expression in spinal cord samples using immunofluorescence (**Figure 2C** and **D**). The expression of CSPGs was mainly concentrated in and around the injury center; it increased in the acute period after SCI and gradually decreased in the sub-acute period. PBM treatment markedly decreased CSPG expression at 3, 7, 14, and 28 dpi in the SCI + PBM group compared with the SCI group. These data suggest that PBM irradiation reduces the accumulation of CSPGs after SCI.

PBM alters the expression of genes involved in glial scar formation in SCI model mice
RNA-seq was performed on the spinal cord tissue in the sham, SCI, and SCI + PBM groups 7 days post-injury, and the expression of 20 target proteoglycan-related genes was analyzed by principal component analysis with gene phenotyping. Principal component analysis identified three dimensions that explained approximately 90.36% of the total gene variation (66.9%, 15.96%, and 7.5% corresponding to dimensions 1–3, respectively) (**Figure 3A** and **B**). Dimension 2 was characterized by most cytokines moving in the same direction (positive correlation loading), whereas dimension 3 was

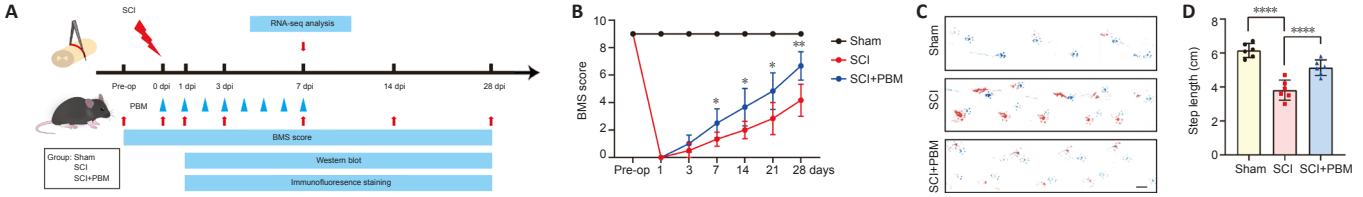

Figure 1 | **Photobiomodulation (PBM) promotes functional recovery after spinal cord injury in mice.**
(A) Experimental design of spinal cord injury (SCI) model construction, PBM irradiation, functional tests, and assays. (B) Basso mouse scale (BMS) score was used to evaluate motor function (n = 6 mice for each group). (C, D) Representative images of footprints and quantification of the step length on day 28 after injury (n = 6 mice for each group). Scale bar: 1 cm. Data are expressed as mean ± SD; the BMS score was analyzed by multiple repeated measuring analysis of variance followed by least significance difference test (*P < 0.05, **P < 0.01, *vs*. SCI group) and the step length was analyzed by one-way analysis of variance with the least significance difference *post hoc* analysis (****P < 0.0001). dpi: Day(s) post-injury.

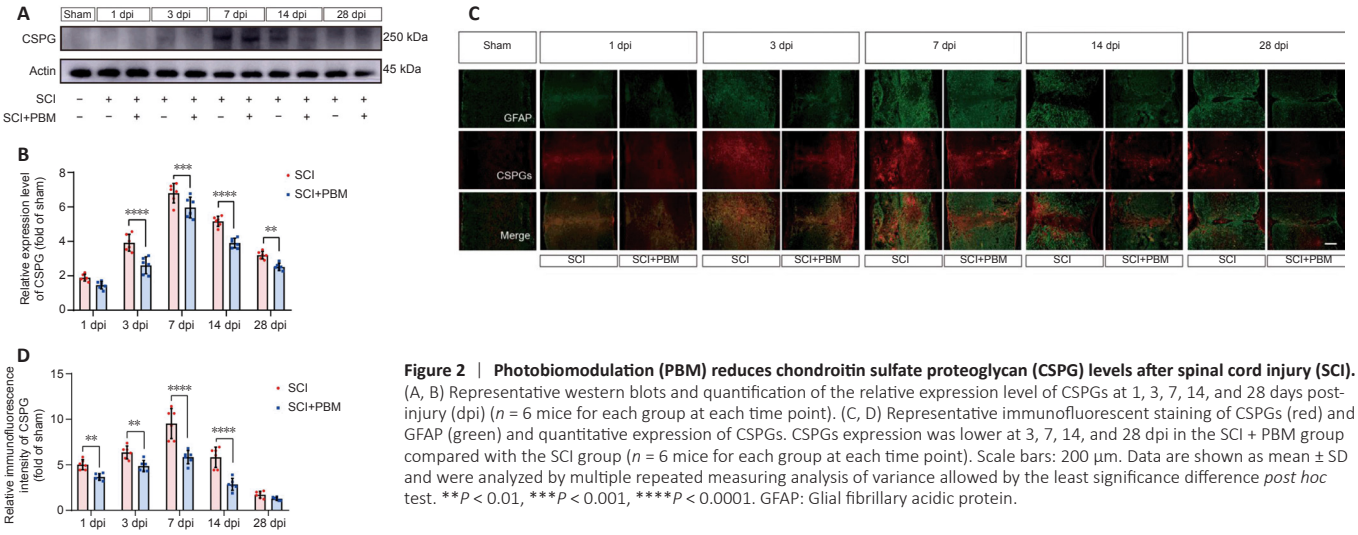

Figure 2 | **Photobiomodulation (PBM) reduces chondroitin sulfate proteoglycan (CSPG) levels after spinal cord injury (SCI).**
(A, B) Representative western blots and quantification of the relative expression level of CSPGs at 1, 3, 7, 14, and 28 days post-injury (dpi) (n = 6 mice for each group at each time point). (C, D) Representative immunofluorescent staining of CSPGs (red) and GFAP (green) and quantitative expression of CSPGs. CSPGs expression was lower at 3, 7, 14, and 28 dpi in the SCI + PBM group compared with the SCI group (n = 6 mice for each group at each time point). Scale bars: 200 μm. Data are shown as mean ± SD and were analyzed by multiple repeated measuring analysis of variance allowed by the least significance difference *post hoc* test. **P < 0.01, ***P < 0.001, ****P < 0.0001. GFAP: Glial fibrillary acidic protein.

characterized by cytokines moving in both positive and negative directions (**Figure 3A**). The component scores were compared between SCI and SCI + PBM groups at 7 days post-injury in dimensions 1 and 2. The two-dimensional plot showed differences in both dimensions (**Figure 3C**), confirming that the expression profile of glial scar-related molecules was markedly modulated by PBM at 7 days post-injury. Heat map of mRNA expression (**Figure 3D** and **E**) and qPCR analysis (**Figure 3F**) showed that the expression of proteoglycan-related genes was greater in the SCI group at 7 days post-injury compared with the sham group and lower in the SCI + PBM group compared with the SCI group. Versican, a type of proteoglycan, was one of the most markedly changed genes and showed higher expression in the SCI group compared with the sham group and lower expression in the SCI + PBM group compared with the SCI group. Together, these data suggest that PBM has a marked effect on gene expression profiles of glial scar factors after SCI.

PBM inhibits the accumulation of versican in mouse spinal cord after SCI

Versican is a widely expressed transitional matrix proteoglycan that plays an important role in biological processes such as developmental morphogenesis and reproduction (McCulloch et al., 2009; Dupuis et al., 2011). Early in the inflammatory process, an increase of versican often coincides with leukocyte invasion. Versican plays a role in promoting the inflammatory response either indirectly through hyaluronic acid or by directly interacting with inflammatory cells (Wight et al., 2020). In multiple sclerosis, versican is one of the CSPGs responsible for repair inhibition and the promotion of local inflammation to exacerbate injury (Ghorbani et al., 2022). We next investigated the changes of versican expression at different time points after SCI. qPCR results showed that compared with the expression level in mice in the Sham group, versican mRNA expression in the SCI group peaked at 7 days post-injury and was gradually downregulated at subsequent time points, and PBM intervention markedly downregulated versican mRNA expression at 3, 7, 14, and 28 days post-injury (**Figure 4A**). Consistent with the qPCR results, western blotting (**Figure 4B** and **C**) and immunofluorescence staining (**Figure 4D** and **E**) also demonstrated that versican expression increased 7 days post-injury and then gradually decreased over 28 days; versican expression was obviously lower in the SCI + PBM group than in the SCI group. These results confirm that versican expression was elevated after injury and markedly down-regulated by PBM irradiation.

PBM inhibits secretion of versican after SCI in astrocytes

Our results suggested that versican might be a key proteoglycan targeted by PBM intervention following SCI. This prompted us to investigate versican-expressing cells that may be targeted by PBM. CSPG is the main component of glial scarring and is secreted by reactive astrocytes after SCI (Bradbury et al., 2002; Silver and Miller, 2004). Our previous study showed that PBM inhibits the inflammatory activation of astrocytes to alleviate the inflammatory response after SCI (Wang et al., 2021b). We next examined the expression of versican in astrocytes after SCI and investigated the effect of PBM intervention on versican expression. The spinal cord tissue in the SCI group was stained with the astrocyte marker GFAP and versican. Versican was detected in astrocytes at 7 days post-injury, and PBM irradiation reduced versican expression (**Figure 5A**). We also performed *in vitro* studies in astrocytes after inflammatory induction. Immunofluorescence (**Figure 5B** and **C**), qPCR (**Figure 5D**), and western blotting (**Figure 5E** and **F**) also showed increased versican expression in astrocytes after inflammation stimulation, and the expression was obviously decreased after PBM intervention. Taken together, these data suggest that PBM is an exogenous stimulus that can reduce the level of versican expression in astrocytes.

The Smad3/Sox9 and MAPK/Sox9 pathways are involved in PBM-mediated regulation of versican expression in astrocytes

Previous studies have suggested that the Smad3/Sox9 and MAPK/Sox9 pathways are involved in the synthesis of CSPGs (Tew and Hardingham, 2006; McKillop et al., 2013; Jahr et al., 2019). To explore the specific mechanisms by which PBM interferes with versican expression in astrocytes, we examined the impact of PBM on these pathways. We administered PBM irradiation to astrocytes after inflammatory stimulation *in vitro* and found that the expression levels of both Sox9 and versican were higher in the inflammation-induced group compared with the control group, whereas the expressions were reduced in the inflammation-induced + PBM group compared with the inflammation-induced group (**Figure 6A** and **B**). The expression levels of p-Smad3, p-P38, and p-Erk1/2 showed the same trends as Sox9, whereas the expression level of p-JNK was not markedly altered after inflammatory stimulation and light intervention. The expression of Smad3, P38, and Erk did not change markedly among the control, inflammation-induced and inflammation-induced + PBM groups (P = 0.5947, Smad3; P = 0.6681, Erk; P = 0.4842, P38). These results indicate that the Smad3/Sox9, P38/Sox9 and Erk/Sox9 pathways, but not the JNK pathway, may be involved in the PBM regulation of versican expression.

To explore the above possibilities, we used SB 202190, FR 180204, and (E)-SIS3 inhibitors to specifically block P38 (**Figure 7A** and **B**), Erk (**Figure 7C** and **D**), and Smad3 (**Figure 7E** and **F**) pathways, respectively, after inflammatory induction of astrocytes. Application of the inhibitors alone reduced the activation of the corresponding pathway molecules and also attenuated the increase in Sox9 and versican expression in response to inflammatory induction. In some cases, PBM exerted stronger inhibitory effects on versican expression compared with the inhibitor compounds, and the combination of PBM and inhibitor tended to enhance the inhibitory effect compared with inhibitors used alone.

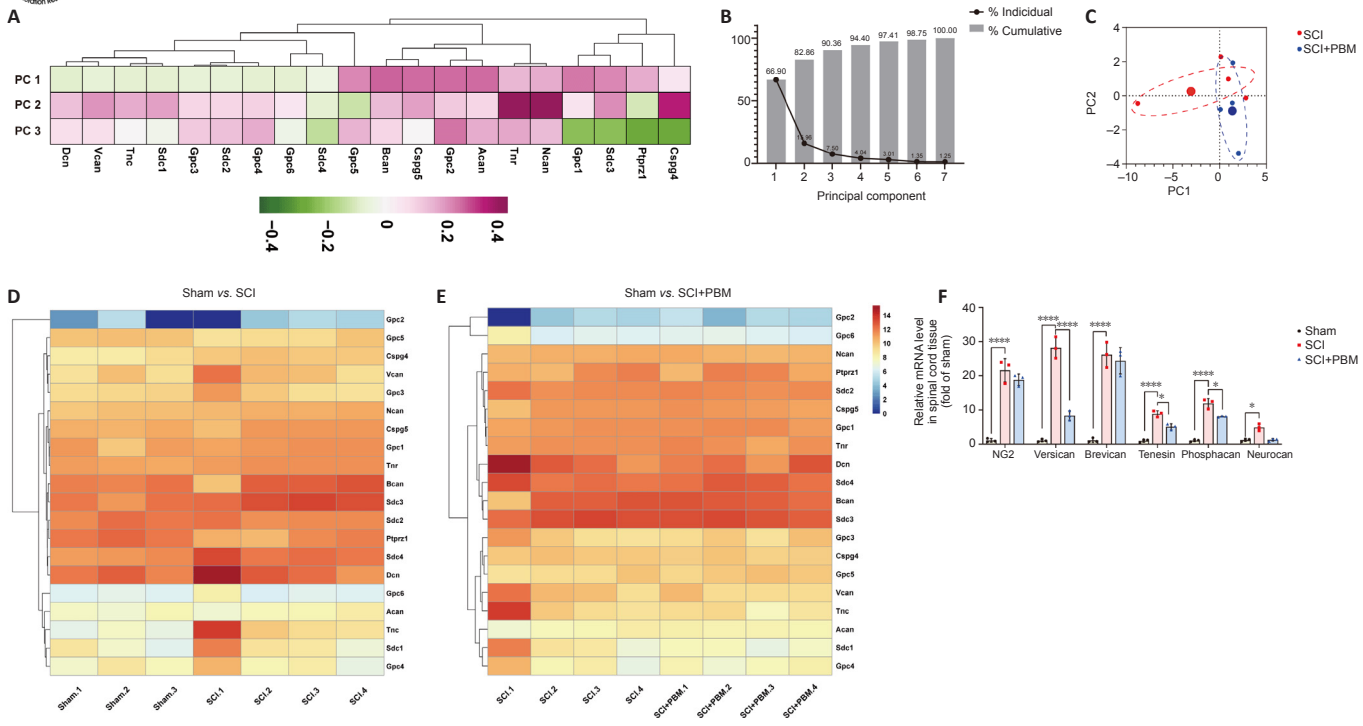

Figure 3 | **Photobiomodulation (PBM) alters gene expressions of glial scar factors in spinal cord injury (SCI) mice.**
(A) Loadings correlation heatmap showed the three main dimensions for gene variation in 20 target proteoglycan-related genes at 7 days post-injury (dpi); dimension 2 was positive for almost all proteoglycan-related genes. (B) Bar graph showing various patterns detected using principal component analysis' principal components 1, 2 and 3 that explained ~90% of the total gene variation. (C) Bidimensional plot of the component scores for every group in principal components 1 and 2 showed differences between SCI and SCI + PBM groups in both principal components 1 and 2. (D, E) Heatmap showing the expression of proteoglycan-related genes upregulated after SCI (D) and downregulated by PBM (E) at 7 dpi. (F) Bar graph showing levels of representative proteoglycan-related genes in the indicated groups (n = 6 mice for each group). Data are shown as mean ± SD and were analyzed by multiple repeated measures analysis of variance with the least significance difference *post hoc* analysis. *P < 0.05, ****P < 0.0001.

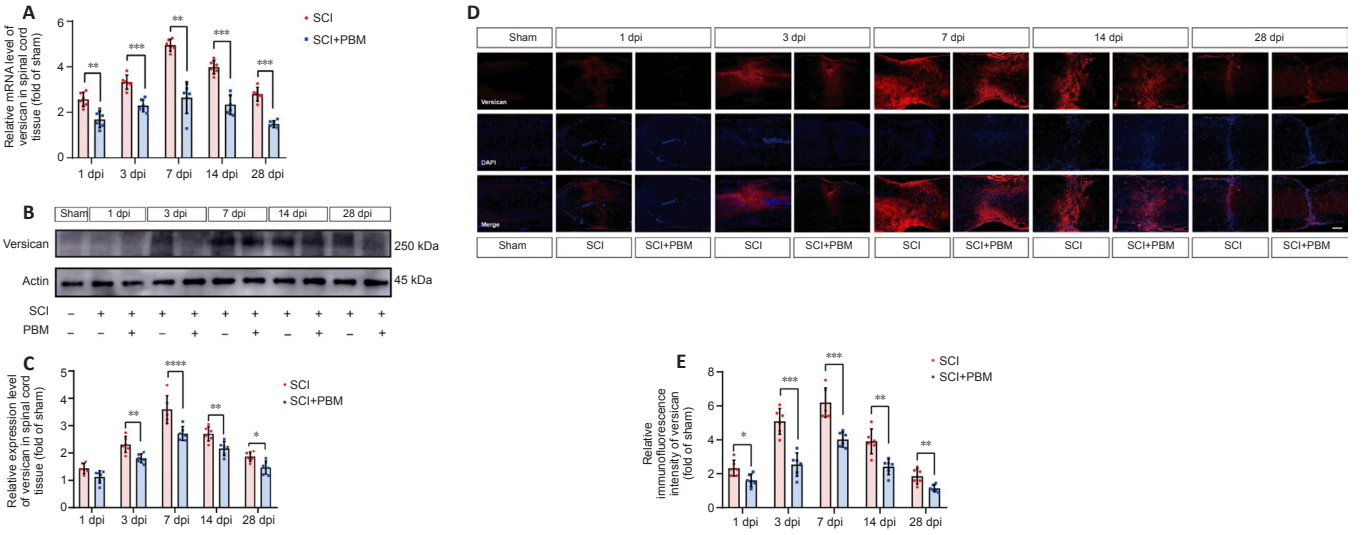

Figure 4 | **Photobiomodulation (PBM) inhibits the accumulation of versican in mice after spinal cord injury (SCI).**
(A) Bar graph showing the relative transcription level of versican in the SCI and SCI + PBM groups at 1, 3, 7, 14, and 28 days post-injury (dpi; n = 6 mice for each group at each time point). (B, C) Representative western blots and quantification of the relative expression level of versican at 1, 3, 7, 14, and 28 dpi (n = 6 mice for each group at each time point). (D, E) Representative immunofluorescent staining of versican (red) and quantification of versican in spinal cord tissue. Versican expression in the SCI group was higher at 3, 7, 14, and 28 dpi compared with expression in the SCI + PBM group (n = 6 mice for each group at each time point). Scale bar: 200 μm. Data are shown as mean ± SD and were analyzed by one-way analysis of variance with the least significance difference *post hoc* analysis. *P < 0.05, **P < 0.01, ***P < 0.001, ****P < 0.0001. DAPI: 4′,6-Diamidino-2-phenylindole.

The Smad3/Sox9 pathway and MAPK/Sox9 pathway are involved in PBM modulation of versican secretion *in vivo*

To further investigate the effects of the Smad3/Sox9 pathway, P38/Sox9 pathway, and Erk/Sox9 pathway on versican expression *in vivo*, mice were intraperitoneally injected with (E)-SIS3, SB 202190, and FR 180204. Activation of the corresponding pathways after SCI was markedly inhibited by intraperitoneal injection of the inhibitor 7 days after injury, similar to the effects of PBM; inhibitor treatment also resulted in inhibited production of versican (**Figure 8A–C**). These results further validate that the Smad3/Sox9 pathway, P38/Sox9 pathway, and Erk/Sox9 pathway are involved in the modulation of versican expression by PBM *in vivo*.

PBM promotes axonal regeneration and increases surviving neurons after SCI through the Smad3/ Sox9 and MAPK/Sox9 pathways

Higher amounts of axonal regeneration were observed in the SCI + PBM, SCI + inhibitors, and SCI + PBM + inhibitors groups compared with the SCI group (**Figure 9A**). The number of surviving neurons was measured within 0.5 mm of the para-lesion area, and the results showed that at 7 days post-injury, the SCI + PBM, SCI + FR 180204, SCI + SB 202190 and SCI + (E)-SIS3 groups had more surviving neurons in the para-lesion area than the SCI group (**Figure 9B** and **C**).

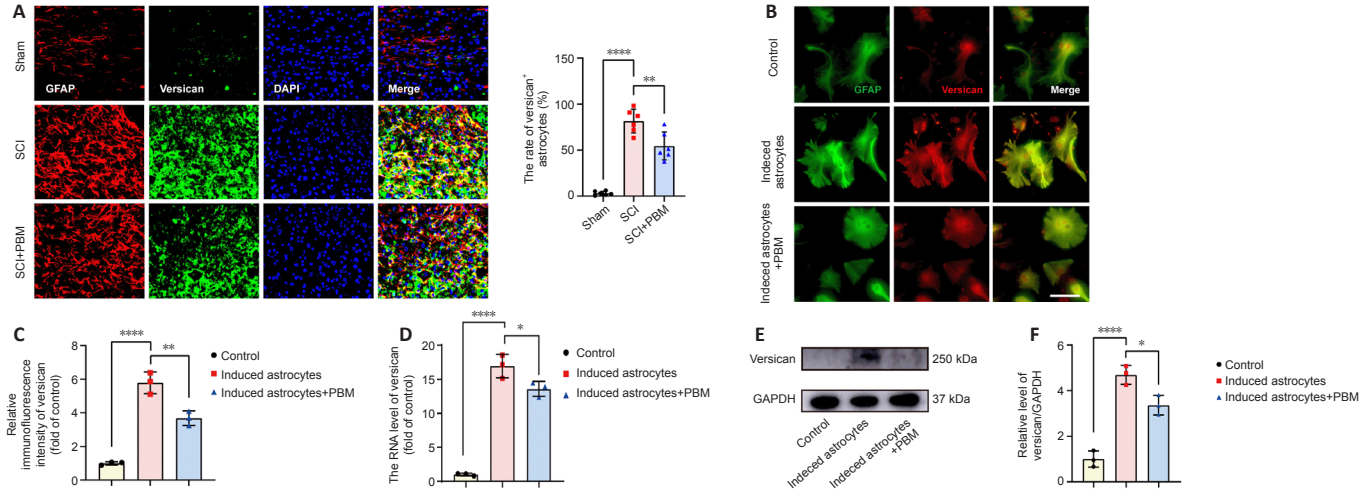

Figure 5 | **Photobiomodulation (PBM) inhibits secretion of versican in astrocytes after spinal cord injury (SCI).**
(A) Representative immunofluorescent staining of versican (green) and GFAP (red) in the epicenter of the lesion area (n = 6 mice for each group at each time point). The co-label rate was larger in the SCI group compared with the Sham group, and the co-label rate was smaller in the SCI + PBM group compared with the SCI group. Scale bar: 200 μm. (B, C) Representative immunofluorescent staining of versican (green) and GFAP (red) and the quantitative expression of versican. Versican expression was markedly higher in SCI group compared with the Sham group and was markedly lower in the SCI + PBM group compared with the SCI group (n = 3 for each group). Scale bar: 50 μm. (D) Bar graph representing the relative transcription level of versican in astrocytes (n = 3 for each group). (E, F) Representative western blots and quantification of the relative expression level of versican in astrocytes (n = 3 for each group). Data are shown as mean ± SD and were analyzed by one-way analysis of variance with the least significance difference *post hoc* analysis. *P < 0.05, **P < 0.01, ****P < 0.0001. DAPI: 4′,6-Diamidino-2-phenylindole; GFAP: glial fibrillary acidic protein.

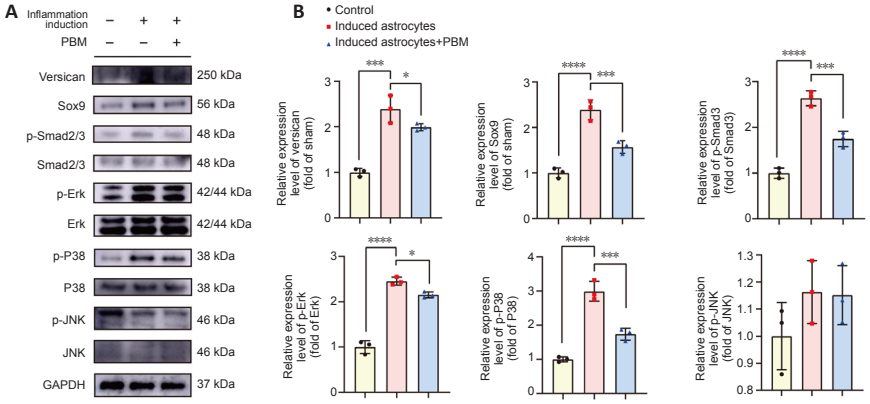

Figure 6 | **PBM modulates the Smad3/Sox9 and MAPK/Sox9 pathways in inflammation-induced astrocytes.**
(A, B) Representative western blots of proteins related to the Smad3/Sox9 pathway, Erk/Sox9 pathway, P38/Sox9 pathway, and JNK/Sox9 pathway in astrocytes and quantification of the relative expression levels of p-Smad3, p-Erk, p-P38, p-JNK, Sox9, and versican. Data are shown as mean ± SD (n = 3 for each group) and were analyzed by multiple repeated measures analysis of variance with least significance difference *post hoc* analysis. *P < 0.05, ***P < 0.001, ****P < 0.0001. Erk: Extracellular signal-regulated kinase; GAPDH: glyceraldehyde-3-phosphate dehydrogenase; JNK: c-Jun N-terminal kinase.

Discussion

CSPGs have been shown to be involved in the inhibition of axonal growth and neuroplasticity after SCI, and modulating the formation of CSPGs has an important role in SCI repair. Here, we reported the inhibitory effects of PBM on the accumulation of CSPGs after SCI. PBM exhibited various effects on the expressions of CSPGs, with the most pronounced inhibitor effects on versican. We further demonstrated that PBM down-regulated the production of versican in astrocytes through the Smad3/Sox9 and MAPK/Sox9 pathways.

In the current study, to verify the modulating effect of subcutaneous irradiation on CSPG formation after SCI, we implanted implantable subcutaneously irradiated laser fibers into male mice after spinal cord contusion injury, an approach we previously developed (Ma et al., 2022). PBM is a reliable treatment for CNS disease and previous experiments have confirmed its therapeutic effects on neurons, macrophages, and astrocytes in *in vitro* models (Huang et al., 2014; Sun et al., 2020; Zhang et al., 2020; Zheng et al., 2021). We previously developed and used biocompatible laser fibers to intervene with SCI *in vivo* and investigated its therapeutic effects and mechanisms (Liang et al., 2020; Wang et al., 2021b; Ma et al., 2022). The fiber irradiation resulted in inhibited inflammatory polarization of macrophages/microglia, reduced reactive activity of astrocytes, alleviated secondary neuroinflammation, and improved neuronal survival and recovery of motor function after SCI (Wang et al., 2021a, b; Ma et al., 2022). In this study, we found that PBM treatment delivered with direct laser fiber irradiation markedly reduced CSPG content in both the acute and subacute phases after injury, which indicates an inhibitory effect of implanted laser fiber irradiation on glial scar formation after SCI.

Trauma to the brain or spinal cord results in the formation of CSPG-rich glial scarring, primarily generated by reactive astrocytes (Silver and Miller, 2004). This dense scar tissue and upregulated CSPGs are thought to be the primary cause of regeneration failure at the site of CNS injury. Modulating the composition of post-injury scarring is considered a viable intervention to promote repair of SCI (Silver and Miller, 2004; Kwok et al., 2012). Grafting biomaterial is used as a substrate for axonal growth and to effectively bypass or modify the inhibitory glial extracellular matrix deposition after SCI (Orr and Gensel, 2018). The use of ChABC to clear and modulate CSPGs has been shown to successfully improve neuro-regeneration and neuroplasticity in various models of CNS injury (Kwok et al., 2011). However, challenges remain in clinical translation, as ChABC is a bacterial enzyme that requires repeated intrathecal injections or continuous pumping into the injury site over time to maintain activity. These invasive manipulations might increase the risk of infection; and improvement in enzyme safety and side effects might require the application of additional techniques (Kwok et al., 2012).

A previous study reported the effect of PBM on reducing glial scarring after SCI, indicating the potential role of PBM in regulation of CSPGs, but the specific modulatory effect of PBM on glial scarring was unknown (Sun et al., 2020). In a study by Janzadeh et al. (2017), 660 nm PBM intervention combined with ChABC enzyme was used to treat micro-vascular clip clamp injury in Wistar rats. PBM irradiation markedly reduced the expression of CSPG in tissues relative to the SCI group, promoting axonal regeneration and facilitating the recovery of motor. In the current study, we examined the modulatory effects of PBM on glial scar components. Our results revealed the effects of PBM on CSPGs, and the modulatory effect on versican was the most pronounced at 7 days post-injury. These findings suggest that PBM has specific effects on CSPGs after SCI, and that versican is a potential target of intervention in post-SCI scarring.

Versican has gained increasing interest in the regulation of inflammatory response after tissue injury as a component of CSPGs (Wight et al., 2014;

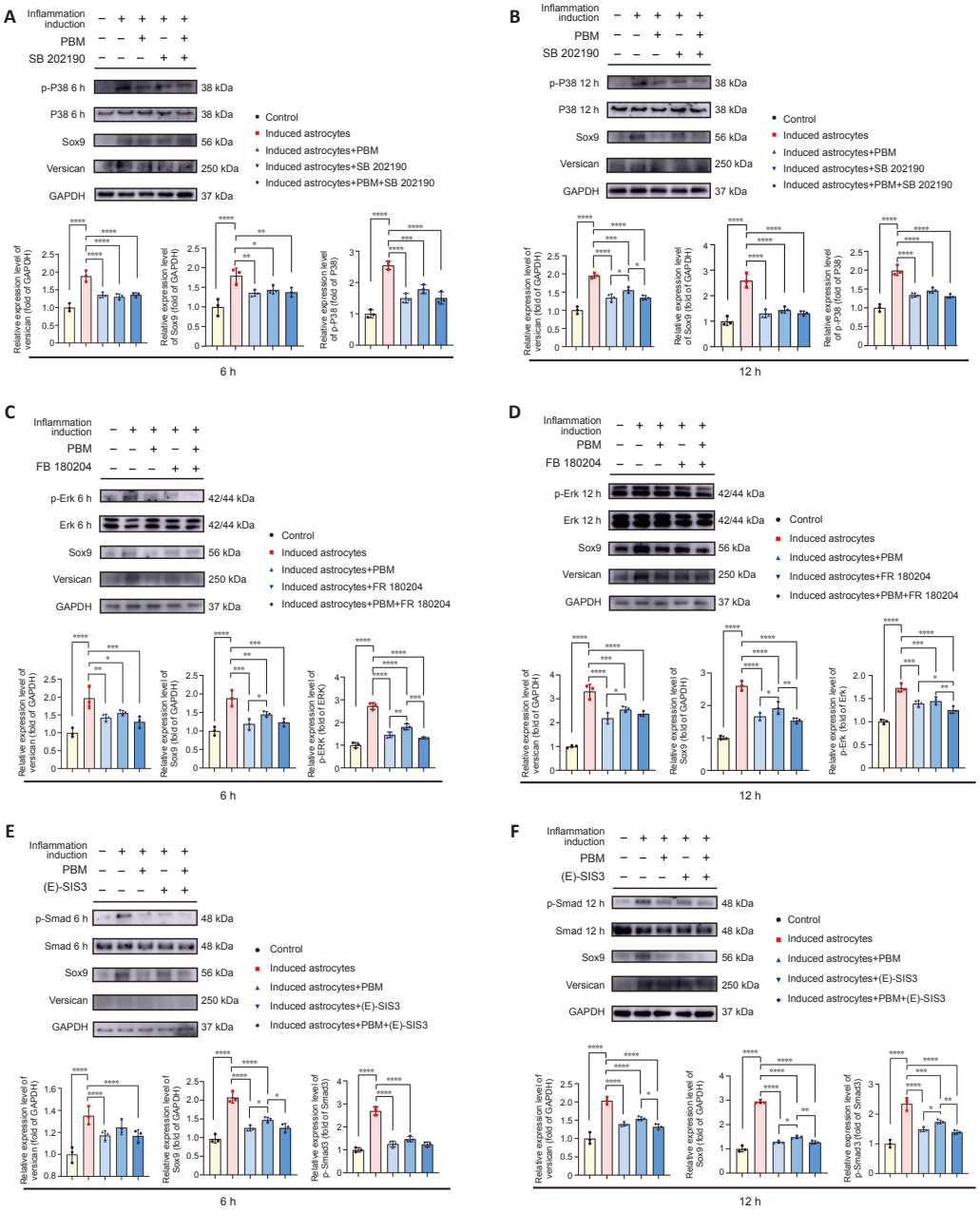

Figure 7 | The P38, Erk and Smad3 pathways are involved in photobiomodulation (PBM) regulation of versican expression in astrocytes.

(A, B) Representative western blots of proteins related to the P38 pathway at 6 and 12 hours after inflammatory induction in astrocytes and quantification of relative expression levels of p-P38, Sox9, and versican (n = 3 for each group). (C, D) Representative western blots of proteins related to the Erk pathway at 6 and 12 hours after inflammatory induction in astrocytes, and quantification of the relative expression levels of p-Erk, Sox9, and versican (n = 3 for each group). (E, F) Representative western blots of proteins related to the Smad3 pathway at 6 and 12 hours after inflammatory induction in the astrocytes, and quantification of the relative expression levels of p-Smad3, Sox9, and versican (n = 3 for each group). Data are shown as mean ± SD and were analyzed by one-way analysis of variance with least significance difference *post hoc* analysis. *P < 0.05, **P < 0.01, ***P < 0.001, ****P < 0.0001. Erk: Extracellular signal-regulated kinase; GAPDH: glyceraldehyde-3-phosphate dehydrogenase.

Wight et al., 2020). Versican is a large CSPG in the CNS that distributes primarily in the extracellular matrix adjacent to myelin fibers during resting; in the pathology process, the expression of versican is increased and causes an unhospitable environment (Asher et al., 2002; Dours-Zimmermann et al., 2009). Astrocytes are involved in glial scar formation after SCI, and thus we investigated whether astrocytes were involved in versican expression after SCI. *In vitro* studies demonstrated a distinct increase in the level of versican expression in astrocytes after inflammatory induction and this expression was downregulated by PBM irradiation or through the suppression of Smad3/Sox9 and MAPK/Sox9 signaling pathways. The expression of versican in astrocytes after SCI has been unclear. A previous study reported that resting astrocytes are not able to produce versican and thus might contribute little to the secretion of versican (Asher et al., 2002). In contrast, in another report demonstrating mice with contusive SCI, the expression of versican was markedly upregulated after injury, and the increased content of versican in astrocytes was comparable to the increased content in all non-astrocytes combined (Anderson et al., 2016). In line with the study by Anderson et al. (2016), we found that astrocytes may play a role in versican production after SCI and in inflammation-induced environment *in vitro*.

We further demonstrated that PBM interferes with astrocyte expression of versican via the Smad3/Sox9 pathway, Erk/Sox9 pathway, and P38/Sox9 pathway. We found that PBM reduced versican secretion from astrocytes cultured *in vitro* following inflammatory stimulation and explored whether Smad3/Sox9 and Erk/Sox9 or P38/Sox9 pathways were involved in versican production. Sox9 is an important transcription factor that plays a key role in mammalian sex determination, chondrogenesis, and nerve injury repair (Eggers et al., 2014). A previous study demonstrated that Sox9 transcriptionally upregulated the expression of *CSPG* genes in astrocytes cultured *in vitro* (Gris et al., 2007) and in the spinal cord of SCI model mice (McKillop et al., 2013). Furthermore, conditional Sox9 clearance reduced CSPG levels in glial scarring and decreased perineuronal net matrix levels around neurons after SCI (McKillop et al., 2013), Sox9 siRNA reduced CSPG production, and activation of the *Sox9* gene in the absence of inflammatory factors using cytomegalovirus (CMV)-Sox9 increased CSPG expression (Yuan et al., 2017). The Smad3/Sox9 pathway is associated with matrix synthesis. A previous study showed that the transforming growth factor-β (TGF-β)/Smad2/3 signaling pathway is involved in the regulation of Sox9 transcription in human chondrocytes (Jahr et al., 2019). Smad3 is associated with Sox9 in a TGF-β-dependent manner and forms a transcriptional complex with Sox9 in the enhancer region of Col2α (Furumatsu et al., 2005; Yang et al., 2016). Furthermore, in astrocytes, Smad proteins are required for TGF-β-mediated expression of CSPGs and modification of related enzyme genes (Susarla et al., 2011). We found that the Smad3/Sox9 pathway was activated in astrocytes following inflammatory stimulation, accompanied by increased versican expression. Furthermore, intraperitoneal administration of E-(SIS), an inhibitor of the Smad3 pathway, resulted in a decrease in versican expression and improvement in axonal regeneration.

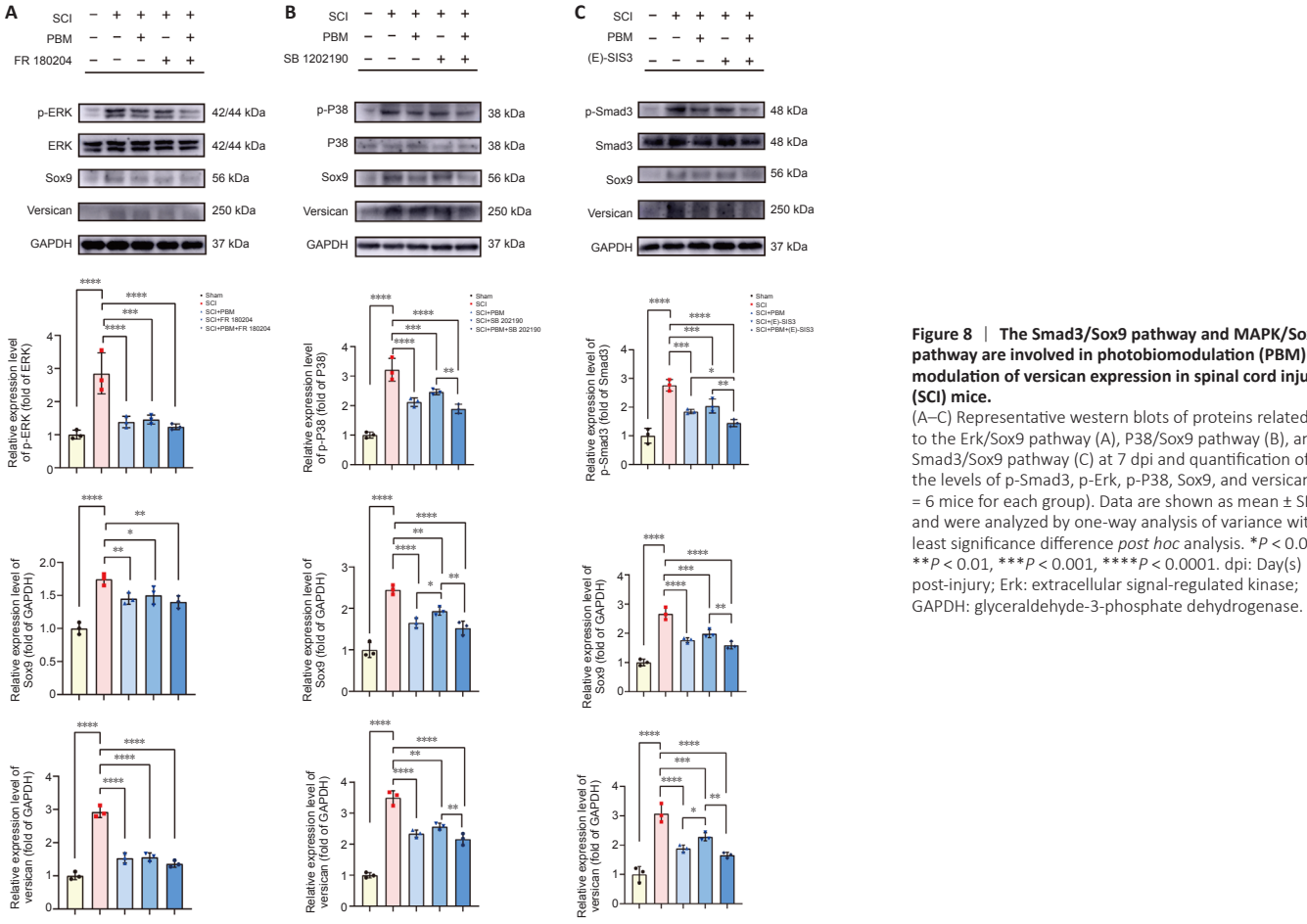

Figure 8 | The Smad3/Sox9 pathway and MAPK/Sox9 pathway are involved in photobiomodulation (PBM) modulation of versican expression in spinal cord injury (SCI) mice.

(A–C) Representative western blots of proteins related to the Erk/Sox9 pathway (A), P38/Sox9 pathway (B), and Smad3/Sox9 pathway (C) at 7 dpi and quantification of the levels of p-Smad3, p-Erk, p-P38, Sox9, and versican (n = 6 mice for each group). Data are shown as mean ± SD and were analyzed by one-way analysis of variance with least significance difference *post hoc* analysis. *P < 0.05, **P < 0.01, ***P < 0.001, ****P < 0.0001. dpi: Day(s) post-injury; Erk: extracellular signal-regulated kinase; GAPDH: glyceraldehyde-3-phosphate dehydrogenase.

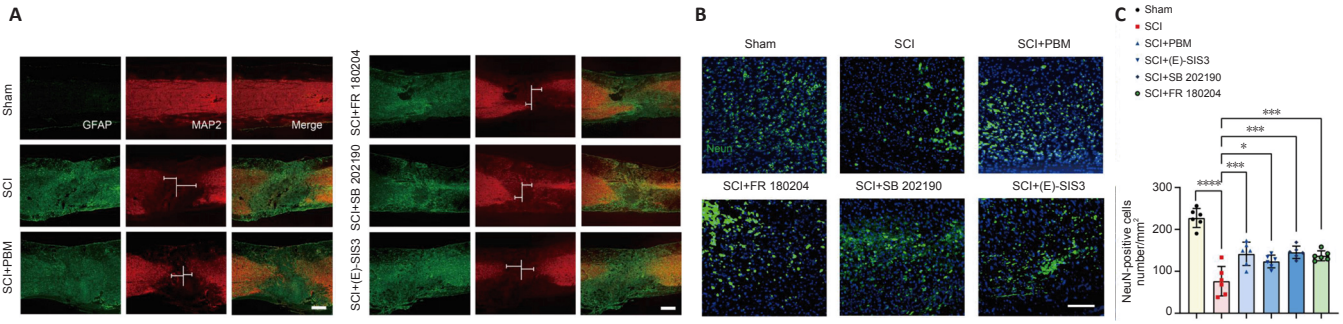

Figure 9 | Photobiomodulation (PBM) promotes axonal regeneration and increases surviving neurons after spinal cord injury (SCI) through the Smad3/Sox9 and MAPK/Sox9 pathways.

(A) Representative images of axon regeneration (marked by MAP2, red) in spinal cord of mice at 7 dpi. Axon regeneration was lower in the SCI group compared with the Sham group and greater in the SCI + PBM group and SCI + inhibitor group compared with the SCI group. The white line in the middle indicates the injury center, and the horizontal white lines show the distance of the axon ending from the injury center. Scale bar: 200 μm. (B, C) Representative immunofluorescence images of surviving neurons in the lesion area 500 μm from the lesion center at 7 dpi (n = 6 mice for each group). The neuron survival rate was lower in the SCI group compared with the Sham group and higher in the SCI + PBM group and SCI + inhibitor group compared with the SCI group. Scale bar: 100 μm. Data are shown as mean ± SD and were analyzed by one-way analysis of variance with least significance difference *post hoc* analysis. *P < 0.05, ***P < 0.001, ****P < 0.0001. dpi: Day(s) post-injury; GFAP: glial fibrillary acidic protein; MAP2: microtubule associated protein 2.

In idiopathic lung fibrosis, Sox9 expression in fibroblasts is upregulated through the MAPK/PI3K-dependent signaling pathway (Gajjala et al., 2021). In an early study involving Sox9 in chondrocyte redifferentiation, post-transcriptional activation of p38 stabilized Sox9 mRNA, which up-regulated Sox9 (Tew and Hardingham, 2006). Additionally, interleukin-1 induces the upregulation of Sox9 expression through physiological activation of p38, and the p38 inhibitor SB202190 reduced Sox9 levels in interleukin-1 experiments (Tew and Hardingham, 2006). In this study, we found that the Erk and P38 levels were up-regulated accompanied with the increased level of Sox9 and versican in SCI model mice, and PBM or Erk or P38 inhibitors suppressed MAPK pathway activation and reduced the expression level of Sox9 and versican.

PBM has been widely used as a therapeutic tool, and previous studies have investigated the effects of PBM on SCI in animal models (Byrnes et al., 2005; Hu et al., 2016; Kazim et al., 2021). PBM irradiation reduces local inflammatory markers, promotes M2 phenotypic polarization of macrophages/microglia, and promotes neuronal survival and axonal regeneration. However, one of the main obstacles to the clinical translation of PBM of SCI is the terminal or treatment dose that can be applied to patients. To investigate the safety parameters of PBM clinical treatment, previous studies have investigated large-bodied animals. Piao et al. (2018, 2019) measured the transmission efficiency of laser light after PBM intervention in dogs using a flexible probe with a miniature photodetector placed in the spinal canal, which measured the efficiency of laser light transmission after PBM intervention in the spinal canal. The detector measured the irradiation intensity of percutaneously irradiated PBM in the spinal canal at nine sites over a length of 8 cm. The results showed that direct skin contact irradiation might be beneficial to improve the therapeutic efficiency of PBM. To address the issue of irradiation parameters and effectiveness, Liang et al. (2020) subcutaneously implanted laser fibers above the injured spinal cord in piglets and verified the safety of PBM irradiation via the laser fiber. In a recent

study, Liang et al. (2022) implanted the subcutaneous irradiation laser fiber on a vertebral fixation rod above the patient's injured spinal cord during the surgical procedure and withdrew the fiber after irradiation. The study demonstrated that *in vivo* PBM irradiation treatment did not produce obvious pathologic changes in patients with SCI. Although the clinical translation of PBM has been explored extensively, further studies are required to evaluate its effectiveness and optimal parameters for clinical application.

This study has several limitations. We showed that inhibiting the expression of versican after SCI by regulating the Sox9 pathway promoted axon regeneration and increased the number of surviving neurons in the para-lesion area. However, the specific mechanism and contribution of versican in SCI recovery still needs to be investigated. Second, our study only examined the effects of PBM on the expression of CSPGs, and versican was only observed in the acute phase with a 7-day irradiation. The effects of irradiation over a longer time need to be investigated in subsequent studies. In addition, we only included male mice in this study, and future experiments in female animals are required.

In conclusion, our study provides some insight into the CSPGs targeted by PBM and the corresponding pathways after SCI, which may contribute to further understanding of the mechanisms of PBM treatment in SCI. Our findings help identify CSPGs that might be involved in the process of SCI and that may represent potential targets for intervention in the SCI pathological environment.

Author contributions: *ZZhang, ZS, ZZhu, XZ, CJ, and XW conceived the idea of investigating the modification of CSPG components after PBM treatment. TW and YM designed the study. LL and ZY performed the in vitro experiments. ZZhu, ZY, and LL performed in vivo experiment. ZZhang, ZS, and JZ wrote the manuscript. BC, TD revised the manuscript. XH and ZW provided guidance for the project to assure the integrity of the work. All authors read and approved the final manuscript.*

Conflicts of interest: *The authors declare no conflicts of interests.*

Data availability statement: *All data relevant to the study are included in the article or uploaded as Additional files.*

Open peer reviewers: *Lorenzo Di Cesare Mannelli, University of Florence, Italy; Xue Yao, Tianjin Medical University, China.*

Additional files:

Additional Table 1: *Irradiation parameters.*

Additional Table 2: *Information of primer sequences.*

Additional Figure 1: *Photobiomodulation (PBM) irradiation alleviated the mechanical allodynia on day 7 post injury in spinal cord injury (SCI) mice.*

Additional file 1: *Open peer review reports 1 and 2.*

References

Anderson MA, Burda JE, Ren Y, Ao Y, O'Shea TM, Kawaguchi R, Coppola G, Khakh BS, Deming TJ, Sofroniew MV (2016) Astrocyte scar formation aids central nervous system axon regeneration. Nature 532:195-200.

Asher RA, Morgenstern DA, Shearer MC, Adcock KH, Pesheva P, Fawcett JW (2002) Versican is upregulated in CNS injury and is a product of oligodendrocyte lineage cells. J Neurosci 22:2225-2236.

Awai L, Bolliger M, Ferguson AR, Courtine G, Curt A (2016) Influence of spinal cord integrity on gait control in human spinal cord injury. Neurorehabil Neural Repair 30:562-572.

Basso DM, Fisher LC, Anderson AJ, Jakeman LB, McTigue DM, Popovich PG (2006) Basso Mouse Scale for locomotion detects differences in recovery after spinal cord injury in five common mouse strains. J Neurotrauma 23:635-659.

Bradbury EJ, Burnside ER (2019) Moving beyond the glial scar for spinal cord repair. Nat Commun 10:3879.

Bradbury EJ, Moon LD, Popat RJ, King VR, Bennett GS, Patel PN, Fawcett JW, McMahon SB (2002) Chondroitinase ABC promotes functional recovery after spinal cord injury. Nature 416:636-640.

Byrnes KR, Waynant RW, Ilev IK, Wu X, Barna L, Smith K, Heckert R, Gerst H, Anders JJ (2005) Light promotes regeneration and functional recovery and alters the immune response after spinal cord injury. Lasers Surg Med 36:171-185.

Chow RT, Johnson MI, Lopes-Martins RA, Bjordal JM (2009) Efficacy of low-level laser therapy in the management of neck pain: a systematic review and meta-analysis of randomised placebo or active-treatment controlled trials. Lancet 374:1897-1908.

Chung H, Dai T, Sharma SK, Huang YY, Carroll JD, Hamblin MR (2012) The nuts and bolts of low-level laser (light) therapy. Ann Biomed Eng 40:516-533.

Dours-Zimmermann MT, Maurer K, Rauch U, Stoffel W, Fässler R, Zimmermann DR (2009) Versican V2 assembles the extracellular matrix surrounding the nodes of ranvier in the CNS. J Neurosci 29:7731-7742.

Dupuis LE, McCulloch DR, McGarity JD, Bahan A, Wessels A, Weber D, Diminich AM, Nelson CM, Apte SS, Kern CB (2011) Altered versican cleavage in ADAMTS5 deficient mice; a novel etiology of myxomatous valve disease. Dev Biol 357:152-164.

Eggers S, Ohnesorg T, Sinclair A (2014) Genetic regulation of mammalian gonad development. Nat Rev Endocrinol 10:673-683.

Francos-Quijorna I, Sánchez-Petidier M, Burnside ER, Badea SR, Torres-Espin A, Marshall L, de Winter F, Verhaagen J, Moreno-Manzano V, Bradbury EJ (2022) Chondroitin sulfate proteoglycans prevent immune cell phenotypic conversion and inflammation resolution via TLR4 in rodent models of spinal cord injury. Nat Commun 13:2933.

Furumatsu T, Tsuda M, Taniguchi N, Tajima Y, Asahara H (2005) Smad3 induces chondrogenesis through the activation of SOX9 via CREB-binding protein/p300 recruitment. J Biol Chem 280:8343-8350.

Gajjala PR, Kasam RK, Soundararajan D, Sinner D, Huang SK, Jegga AG, Madala SK (2021) Dysregulated overexpression of Sox9 induces fibroblast activation in pulmonary fibrosis. JCI Insight 6:e152503.

Gaudet AD, Fonken LK, Ayala MT, Maier SF, Watkins LR (2021) Aging and miR-155 in mice influence survival and neuropathic pain after spinal cord injury. Brain Behav Immun 97:365-370.

Ghorbani S, Jelinek E, Jain R, Buehner B, Li C, Lozinski BM, Sarkar S, Kaushik DK, Dong Y, Wight TN, Karimi-Abdolrezaee S, Schenk GJ, Strijbis EM, Geurts J, Zhang P, Ling CC, Yong VW (2022) Versican promotes T helper 17 cytotoxic inflammation and impedes oligodendrocyte precursor cell remyelination. Nat Commun 13:2445.

Ghosh S, Chan CK (2016) Analysis of RNA-Seq data using TopHat and Cufflinks. Methods Mol Biol 1374:339-361.

Gris P, Tighe A, Levin D, Sharma R, Brown A (2007) Transcriptional regulation of scar gene expression in primary astrocytes. Glia 55:1145-1155.

Hu D, Zhu S, Potas JR (2016) Red LED photobiomodulation reduces pain hypersensitivity and improves sensorimotor function following mild T10 hemicontusion spinal cord injury. J Neuroinflammation 13:200.

Hu J, Jin LQ, Selzer ME (2022) Inhibition of central axon regeneration: perspective from chondroitin sulfate proteoglycans in lamprey spinal cord injury. Neural Regen Res 17:1955-1956.

Huang YY, Nagata K, Tedford CE, Hamblin MR (2014) Low-level laser therapy (810 nm) protects primary cortical neurons against excitotoxicity in vitro. J Biophotonics 7:656-664.

Hutson TH, Di Giovanni S (2019) The translational landscape in spinal cord injury: focus on neuroplasticity and regeneration. Nat Rev Neurol 15:732-745.

Jahr H, Gunes S, Kuhn AR, Nebelung S, Pufe T (2019) Bioreactor-controlled physoxia regulates TGF-β signaling to alter extracellular matrix synthesis by human chondrocytes. Int J Mol Sci 20:1715.

Janzadeh A, Sarveazad A, Yousefifard M, Dameni S, Samani FS, Mokhtarian K, Nasirinezhad F (2017) Combine effect of chondroitinase ABC and low level laser (660nm) on spinal cord injury model in adult male rats. Neuropeptides 65:90-99.

Kazim SF, Bowers CA, Cole CD, Varela S, Karimov Z, Martinez E, Ogulnick JV, Schmidt MH (2021) Corticospinal motor circuit plasticity after spinal cord injury: harnessing neuroplasticity to improve functional outcomes. Mol Neurobiol 58:5494-5516.

Khalil AS, Hellenbrand D, Reichl K, Umhoefer J, Filipp M, Choe J, Hanna A, Murphy WL (2022) A localized materials-based strategy to non-virally deliver chondroitinase ABC mRNA improves hindlimb function in a rat spinal cord injury model. Adv Healthc Mater 11:e2200206.

Kong F, Sun K, Zhu J, Li F, Lin F, Sun X, Luo X, Ren C, Lu L, Zhao S, Sun J, Wang Y, Shi J (2021) PD-L1 improves motor function and alleviates neuropathic pain in male mice after spinal cord injury by inhibiting MAPK pathway. Front Immunol 12:670646.

Kwok JC, Warren P, Fawcett JW (2012) Chondroitin sulfate: a key molecule in the brain matrix. Int J Biochem Cell Biol 44:582-586.

Kwok JC, Dick G, Wang D, Fawcett JW (2011) Extracellular matrix and perineuronal nets in CNS repair. Dev Neurobiol 71:1073-1089.

Li L, Ni L, Eugenin EA, Heary RF, Elkabes S (2019) Toll-like receptor 9 antagonism modulates astrocyte function and preserves proximal axons following spinal cord injury. Brain Behav Immun 80:328-343.

Liang Z, Lei T, Wang S, Li P, Chen B, Pan D, Zhang Y, Zuo X, Wang X, Luo Z, Hu X, Ding T, Wang Z (2022) Clinical safety study of photobiomodulation in acute spinal cord injury by scattering fiber. Lasers Med Sci 37:3433-3442.

Liang Z, Lei T, Wang S, Zuo X, Li K, Song J, Sun J, Zhang J, Zheng Q, Kang X, Ma Y, Hu X, Ding T, Wang Z (2020) Photobiomodulation by diffusing optical fiber on spinal cord: A feasibility study in piglet model. J Biophotonics 13:e201960022.

Livak KJ, Schmittgen TD (2001) Analysis of relative gene expression data using real-time quantitative PCR and the 2(-Delta Delta C(T)) method. Methods 25:402-408.

Lorenzini L, Giuliani A, Giardino L, Calzà L (2010) Laser acupuncture for acute inflammatory, visceral and neuropathic pain relief: An experimental study in the laboratory rat. Res Vet Sci 88:159-165.

Ma M, Basso DM, Walters P, Stokes BT, Jakeman LB (2001) Behavioral and histological outcomes following graded spinal cord contusion injury in the C57Bl/6 mouse. Exp Neurol 169:239-254.

Ma Y, Li P, Ju C, Zuo X, Li X, Ding T, Liang Z, Zhang J, Li K, Wang X, Zhu Z, Zhang Z, Song Z, Quan H, Hu X, Wang Z (2022) Photobiomodulation attenuates neurotoxic polarization of macrophages by inhibiting the Notch1-HIF-1α/NF-κB signalling pathway in mice with spinal cord injury. Front Immunol 13:816952.

McCulloch DR, Nelson CM, Dixon LJ, Silver DL, Wylie JD, Lindner V, Sasaki T, Cooley MA, Argraves WS, Apte SS (2009) ADAMTS metalloproteases generate active versican fragments that regulate interdigital web regression. Dev Cell 17:687-698.

McKillop WM, Dragan M, Schedl A, Brown A (2013) Conditional Sox9 ablation reduces chondroitin sulfate proteoglycan levels and improves motor function following spinal cord injury. Glia 61:164-177.

Micheli L, Cialdai F, Pacini A, Branca JJV, Morbidelli L, Ciccone V, Lucarini E, Ghelardini C, Monici M, Di Cesare Mannelli L (2019) Effect of NIR laser therapy by MLS-MiS source against neuropathic pain in rats: in vivo and ex vivo analysis. Sci Rep 9:9297.

Moon LD, Asher RA, Rhodes KE, Fawcett JW (2001) Regeneration of CNS axons back to their target following treatment of adult rat brain with chondroitinase ABC. Nat Neurosci 4:465-466.

Mukherjee N, Nandi S, Garg S, Ghosh S, Ghosh S, Samat R, Ghosh S (2020) Targeting chondroitin sulfate proteoglycans: an emerging therapeutic strategy to treat CNS injury. ACS Chem Neurosci 11:231-232.

Orr MB, Gensel JC (2018) Spinal cord injury scarring and inflammation: therapies targeting glial and inflammatory responses. Neurotherapeutics 15:541-553.

Percie du Sert N, Hurst V, Ahluwalia A, Alam S, Avey MT, Baker M, Browne WJ, Clark A, Cuthill IC, Dirnagl U, Emerson M, Garner P, Holgate ST, Howells DW, Karp NA, Lazic SE, Lidster K, MacCallum CJ, Macleod M, Pearl EJ, et al. (2020) The ARRIVE guidelines 2.0: Updated guidelines for reporting animal research. PLoS Biol 18:e3000410.

Piao D, Sypniewski LA, Bailey C, Dugat D, Burba DJ, De Taboada L (2018) Flexible nine-channel photodetector probe facilitated intraspinal multisite transcutaneous photobiomodulation therapy dosimetry in cadaver dogs. J Biomed Opt 23:1-4.

Piao D, Sypniewski LA, Dugat D, Bailey C, Burba DJ, DeTaboada L (2019) Transcutaneous transmission of photobiomodulation light to the spinal canal of dog as measured from cadaver dogs using a multi-channel intra-spinal probe. Lasers Med Sci 34:1645-1654.

Salehpour F, Mahmoudi J, Kamari F, Sadigh-Eteghad S, Rasta SH, Hamblin MR (2018) Brain photobiomodulation therapy: a narrative review. Mol Neurobiol 55:6601-6636.

Schneider CA, Rasband WS, Eliceiri KW (2012) NIH Image to ImageJ: 25 years of image analysis. Nat Methods 9:671-675.

Shen Y, Tenney AP, Busch SA, Horn KP, Cuascut FX, Liu K, He Z, Silver J, Flanagan JG (2009) PTPsigma is a receptor for chondroitin sulfate proteoglycan, an inhibitor of neural regeneration. Science 326:592-596.

Silver J, Miller JH (2004) Regeneration beyond the glial scar. Nat Rev Neurosci 5:146-156.

Sofroniew MV, Vinters HV (2010) Astrocytes: biology and pathology. Acta Neuropathol 119:7-35.

Sun J, Zhang J, Li K, Zheng Q, Song J, Liang Z, Ding T, Qiao L, Zhang J, Hu X, Wang Z (2020) Photobiomodulation therapy inhibit the activation and secretory of astrocytes by altering macrophage polarization. Cell Mol Neurobiol 40:141-152.

Susarla BT, Laing ED, Yu P, Katagiri Y, Geller HM, Symes AJ (2011) Smad proteins differentially regulate transforming growth factor-β-mediated induction of chondroitin sulfate proteoglycans. J Neurochem 119:868-878.

Tew SR, Hardingham TE (2006) Regulation of SOX9 mRNA in human articular chondrocytes involving p38 MAPK activation and mRNA stabilization. J Biol Chem 281:39471-39479.

Tran AP, Warren PM, Silver J (2018) The biology of regeneration failure and success after spinal cord injury. Physiol Rev 98:881-917.

Walker JM (1994) The bicinchoninic acid (BCA) assay for protein quantitation. Methods Mol Biol 32:5-8.

Wang X, Zhang Z, Zhu Z, Liang Z, Zuo X, Ju C, Song Z, Li X, Hu X, Wang Z (2021a) Photobiomodulation promotes repair following spinal cord injury by regulating the transformation of A1/A2 reactive astrocytes. Front Neurosci 15:768262.

Wang X, Li X, Zuo X, Liang Z, Ding T, Li K, Ma Y, Li P, Zhu Z, Ju C, Zhang Z, Song Z, Quan H, Zhang J, Hu X, Wang Z (2021b) Photobiomodulation inhibits the activation of neurotoxic microglia and astrocytes by inhibiting Lcn2/JAK2-STAT3 crosstalk after spinal cord injury in male rats. J Neuroinflammation 18:256.

Wight TN, Kang I, Merrilees MJ (2014) Versican and the control of inflammation. Matrix Biol 35:152-161.

Wight TN, Kang I, Evanko SP, Harten IA, Chang MY, Pearce OMT, Allen CE, Frevert CW (2020) Versican-A critical extracellular matrix regulator of immunity and inflammation. Front Immunol 11:512.

Yang H, Yuan C, Wu C, Qian J, Shi Q, Li X, Zhu X, Zou J (2016) The role of TGF-β1/Smad2/3 pathway in platelet-rich plasma in retarding intervertebral disc degeneration. J Cell Mol Med 20:1542-1549.

Yang S, Yan JL (2022) Effects of SOX9 on chondrocyte differentiation. Zhongguo Zuzhi Gongcheng Yanjiu 26:2279-2284.

Yu SS, Li ZY, Xu XZ, Yao F, Luo Y, Liu YC, Cheng L, Zheng MG, Jing JH (2022) M1-type microglia can induce astrocytes to deposit chondroitin sulfate proteoglycan after spinal cord injury. Neural Regen Res 17:1072-1079.

Yuan J, Liu W, Zhu H, Chen Y, Zhang X, Li L, Chu W, Wen Z, Feng H, Lin J (2017) Curcumin inhibits glial scar formation by suppressing astrocyte-induced inflammation and fibrosis in vitro and in vivo. Brain Res 1655:90-103.

Zhang J, Sun J, Zheng Q, Hu X, Wang Z, Liang Z, Li K, Song J, Ding T, Shen X, Zhang J, Qiao L (2020) Low-level laser therapy 810-nm up-regulates macrophage secretion of neurotrophic factors via PKA-CREB and promotes neuronal axon regeneration in vitro. J Cell Mol Med 24:476-487.

Zheng Q, Zhang J, Zuo X, Sun J, Liang Z, Hu X, Wang Z, Li K, Song J, Ding T, Shen X, Ma Y, Li P (2021) Photobiomodulation promotes neuronal axon regeneration after oxidative stress and induces a change in polarization from M1 to M2 in macrophages via stimulation of CCL2 in neurons: relevance to spinal cord injury. J Mol Neurosci 71:1290-1300.

P-Reviewers: Di Cesare Mannelli L, Yao X; C-Editor: Zhao M; S-Editors: Yu J, Li CH; L-Editors: Yu J, Song LP; T-Editor: Jia Y

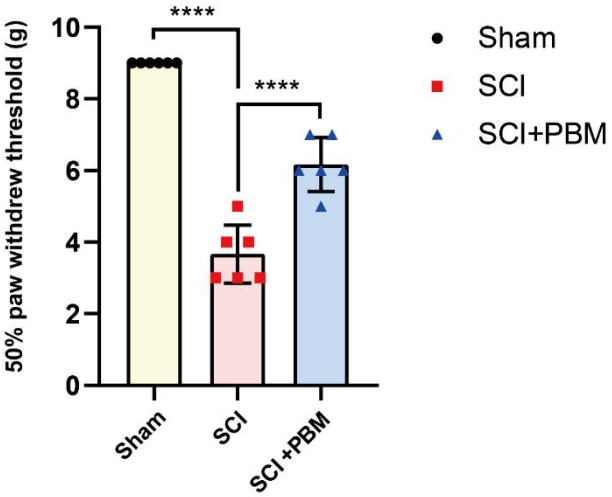

Additional Figure 1 Photobiomodulation (PBM) irradiation alleviated the mechanical allodynia on day 7 post injury in spinal cord injury (SCI) mice.

Data are shown as mean ± SD (n = 6 for each group), and were analyzed by one-way analysis of variance with least significance difference post hoc analysis. ****P < 0.0001.

Additional Table 1 Irradiation parameters

Equipment parameters	Irradiation value for rats	
	In vivo	***In vitro***
Center wavelength (nm)	810	810
Spectral bandwidth (nm)	< 3	< 3
Operation mode	Continuous mode	Continuous mode
Irradiation power (mW)	50	150
Irradiation time (min)	50	8
Irradiation energy (J)	150	72
Irradiation frequency	1/d	2/d
Treatment schedule (days)	7	0.5-1

Additional Table 2 Information of primer sequences

Gene	Forward primer sequence (5'– 3')	Reverse primer sequence (5'– 3')
NG2	TCTTACCTTGGCCCTGTTGG	ACTCTGGTCAGAGCTGAGGG
Versican	GCAGATTTGATGCCTACTGC	ACGGAGTAGTTGTTACATCCG
Brevican	GTGGAGTGGCTGTGGCTC	AACATAGGCAGCGGAAACC
Tenascin	ACCATGCTGAGATAGATGTTCCAAA	CTTGACAGCAGAAACACCAATCC
Phosphacan	GCCGGGAGTCTTCACTGACATT	TTCTCTTCCTGCCTTGTGCTGA
Neurocan	CAACACAGGACTGCAATATG	TATAGGGTAGGTTGTAGTTGC
β-Actin	TGTTACCAACTGGGACGACA	GGGGTGTTGAAGGTCTCAAA